Electric Control of a Phononic Crystal constituted of Piezoelectric Layers using Schottky Diode

Massaï Hatoumva, Emmanuel Siryabe, Pierre Maréchal, Joseph Y Effa, Gambo Betchewe

Electric Control of a Phononic Crystal constituted of Piezoelectric Layers using Schottky Diode

To cite this article before publication: Massaï Hatoumva *et al* 2022 *Smart Mater. Struct.* in press https://doi.org/10.1088/1361-665X/aca454

Electric Control of a Phononic Crystal constituted of Piezoelectric Layers using Schottky Diode.

Massaï HATOUMVA[1], Emmanuel SIRYABE[2], Pierre MARÉCHAL[3], Joseph Yves EFFA[4], Gambo BETCHEWE[1]

[1] *Faculty of Sciences, Department of Physics, The University of Maroua, P.O.Box 814 Maroua, Cameroon.*
[2] *Safran Helicopter Engines, Groupe Evaluation Non Destructive, Avenue Joseph Szydlowski, 64511 Bordes, France.*
[3] *Laboratoire Ondes et Milieux Complexes (LOMC), UMR 6294 CNRS, Université du Havre, Le Havre, France.*
[4] *Electronique, Electrotechnique et Automatisme (EEA), Department of Physics, Faculty of Sciences, The University of Ngaoundéré, P.O.Box 454 Ngaoundéré, Cameroon.*

Abstract

A one-dimensional piezoelectric phononic crystal (PPC) consisting of a periodic pattern made of two perfectly bonded materials: one active (piezoelectric), the other passive (elastic) and exhibiting a strong acoustic impedance contrast is studied. We are interested in the tunability of piezoelectric inclusions in order to control the propagation of ultrasonic waves in the MHz range from a nonlinear electrical component connected to the terminals of the piezoelectric elements. After modeling the dynamic resistance of the Schottky diode, based on the piezoelectricity equations, a one-dimensional analytical model is proposed to take into account the resistive impedance effect of this diode connected to the electrodes of the active plate. Thus, we have shown that the application of various electrical boundary conditions (EBCs) on the electrodes (open-circuit, short-circuit, connecting an electrical load) allows to change the effective properties of the piezoelectric plate in particular and those of the PPC in general. The dispersion of the waves is then electrically tuned and, depending on the applied EBCs, we have demonstrated numerically the possibility of opening Bragg or hybridization gaps in the PPC band structure.

Keywords: Piezoelectric Phononic Crystal, Tunability, Schottky diode, Dynamic resistance, Electric impedance, Ultrasonic waves.

1 Introduction

Like materials which have the properties of absorbing ultrasonic waves in a given frequency range, it is possible to design artificial materials made up of periodic networks of inclusions in one, two or three dimensions and which can strongly act on the propagation of acoustic waves. These materials are generally referred to as Phononic Crystals (PCs) [1]. The rise of PCs in various fields of application such as electronics, seismics or imaging [2], is mainly due to the exceptional properties that these structures have for controlling the propagation of elastic waves [3]. However, due to the fixed properties imposed by the constituent materials at the fabrication stage, these applications are very limited. Thus, a change in these geometric and/or physical properties makes it possible to modulate the spectral properties of such a structure. In other words, this consists in changing the dispersion of the waves by shifting frequency band gaps. As a result, different approaches have been proposed, for example by modifying the orientation of parallelepipedal inclusions within a PC [4]. Other studies have been carried out on the control of band structures in two-dimensional waveguides [5]. Jim *et al.* [6] studied the influence of temperature on the band structure in ferroelectric ceramic/epoxy phononic crystal. In addition, the studies performed on the active control of the propagation of bending acoustic waves on beams have shown that the adaptation of the connectivity of piezoelectric materials bonded to a beam, brings significant changes to its structure of forbidden bands [7, 8]. However, the practical implementation of all these methods poses problems. Solutions based on an external control of the properties of the PC were then proposed. These solutions are based on the use of active materials, such as electrostrictive [9], magnetostrictive [10, 11] or piezoelectric [5, 12, 13] materials. Among these different possibilities, those offering the greatest stability and simplicity of implementation are those in which the active elements are piezoelectric. In order to optimize the efficiency of wave control, recent works have focused on the frequency tunability of PPCs. In particular by inserting active materials, without having to change the geometry of the PC, it has been shown that it is possible to modulate the frequency position or the width of the Bragg or hybridization forbidden bands by an external control of the properties of the piezoelectric plate. The presented work is situated in the global context of the existing research in electrically loaded or driven piezoactive phononic structures. This tuning method offers the advantage of being possibly driven by programmable controllers [14, 15]. Among the reference works dealing with the tunability of piezoelectric phononic crystals, some works have investigated the effect of a passive electrical load. They have shown that it is possible to considerably modulate the properties of a PC made up of alternating piezoelectric and elastic layers by modifying the electrical boundary conditions of active inclusions. The case of the connexion of an electrical passive load across the piezoelectric element has been investigated, with an electrical open-circuit or short-circuit by S.A. Mansoura *et al.* [16, 17] in the case of bulk waves and by C. Vasseur *et al.* [18] in the case of guided waves, and with resistive loads by L. Airoldi *et al.* [19]. Frequency dependant electrical load have also been investigated with a capacitance by S. Degraeve *et al.* [20, 21, 22] and M.F. Ponge *et al.* [23, 24], with an inductance by S.A. Mansoura *et al.* [25], and with a resonant parallel LC load by E.A. Flores-Parra *et al.* [26]. The case of active loads has also been explored with the case of study of a negative resistance by Zeng *et al.* [27], and that of a negative capacitance by S.A. Mansoura *et al.* [28]. In those active loads, semiconductor devices do play a role, but the effect of an electrical diode as an electrically driven load constitutes a potential novelty, and requires to be investigated as a promising flexible and robust tuning device. The key parameters for the spectral study of the pass bands and stop bands of such structures are : the acoustic impedance contrast, the ratio between the plates thickness and the wavelength [29]. Thus, with the aim of numerically evaluating the contribution of a nonlinear electrical component in the tunability of PPCs and developing new functionalities in order to broaden their application field, we are focusing on the addition of a diode on the active element and its consequences on the propagation of ultrasonic waves in the PPC. The use of a nonlinear electrical component such as the diode is motivated by the desire to easily integrate it into the heart of a circuit for a specific function: that of boosting the performance of tunable PPCs. To do this, we study in practice a statically biased Schottky diode by applying an alternative component to it, in order to model its variable dynamic resistance, as highlighted by Kalinin *et al.* [30]. Its advantages over conventional P-N junction diodes is that it has very short switching times and much lower losses. Thanks to its nonlinear behavior, the Schottky diode constitutes the cornerstone

of detection circuits, frequency multipliers or even mixers in the high frequency bands (THz) [31]. Traditionally, these diodes have been manufactured using silicon technology because it is a mature and reliable technology [32, 33]. After having modeled the dynamic resistance of the Schottky diode and established the wave dispersion equation according to the Bloch-Floquet approach [21, 22, 34], we study in the MHz frequency range a finite periodic structure based on a piezoelectric/elastic bilayer. The influence of electric charges of the diode on the band structure of the considered PPC is evaluated and discussed.

2 Schottky diode model and characteristic curves

2.1 *Electrical modeling of the resistance of a Schottky's diode*

The Schottky diode is a component largely controlled by the metal/semiconductor interface and the management of boundary conditions (Schottky and ohmic contact) constitutes a key step in the modeling of the device [30]. The basic structure of a Schottky diode is shown in Figure 1(a) and its equivalent circuit diagram commonly used for frequencies up to a few hundred GHz [35] in Figure 1(b).

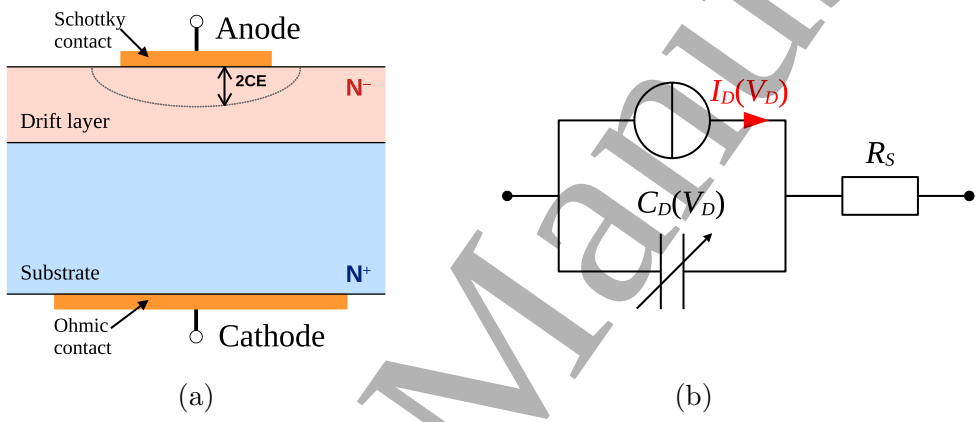

Figure 1: (a) Basic structure of a Schottky diode, (b) Equivalent electric circuit.

The Schottky contact is modeled by a current source $I_D(V_D)$ in parallel with a nonlinear capacitor $C_D(V_D)$ and a series resistance R_S. As long as the bias voltage is not too high, we can assume that the dynamic resistance R_D is very large compared to the series resistance R_S [30]. In dynamic regime, the current source can be represented by a dynamic resistance $R_D(V_D)$ such as:

$$R_D = \frac{\partial V_D}{\partial I_D}. \tag{1}$$

From the thermionic emission model [36], the expression of $I_D(V_D)$ giving the diode current-voltage equation is defined by:

$$I_D = I_S.\left(\exp\left(\frac{V_D}{nV_T}\right) - 1\right), \tag{2}$$

where $V_T = kT/q$, and $\{n, k, T, q\}$ are described in Table 1, *i.e.*

$$V_D = nV_T \ln\left(\frac{I_D}{I_S} + 1\right). \tag{3}$$

Dividing equation (3) by equation (2) lead to the expression of R_S:

$$R_S(V_D) = \frac{V_D}{I_S.\left(\exp\left(\frac{V_D}{nV_T}\right) - 1\right)}. \tag{4}$$

Inserting equations (3) and (2) into equation (1) and taking the first derivative of V_D with respect to I_D lead to the expression of the dynamic resistance R_D:

$$R_D(V_D) = \frac{nV_T}{I_S} \exp\left(\frac{-V_D}{nV_T}\right), \tag{5}$$

with I_S the reverse saturation current, n the non-ideality factor, q the electronic charge, k the Boltzmann's constant and T the absolute temperature [36]. In the following, the resistance of a diode (equation (5))is studied with the analytical definition of the electrical dynamic resistance load R_D.

2.2 *Schottky diode characteristics*

The n, q, k, I_S, T and V_T values used for plotting the $I_D(V_D)$ and $R_D(V_D)$ characteristics (Figure 2) of the reference diode based on SiC are summarized in Table 1.

Table 1: Characteristic properties of the diode [36].

n	$q(C)$	$k(J/K)$	$I_S(A)$	$T(K)$	$V_T(mV)$
1.29	1.6×10^{-19}	1.38×10^{-23}	10^{-9}	293	25

n : non-ideality factor (dimensionless) ; q : electronic charge ;
k : Boltzmann's constant ; I_S : reverse saturation current ;
T : absolute temperature ; V_T : thermal voltage at room temperature.

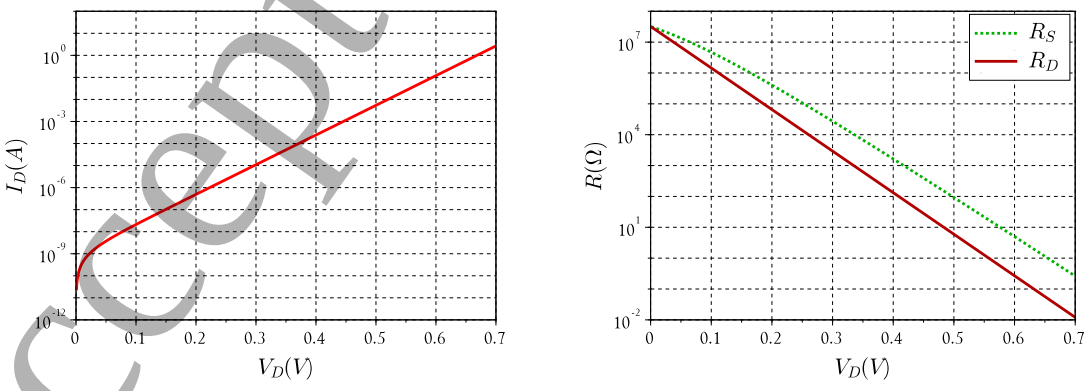

Figure 2: Diode 1N4148 (a) Current-voltage characteristic; (b) Resistance versus voltage characteristic.

Figure 2(a) displays that the exponential law is verified in log scale, this corresponds to the forward bias of the diode, thus allowing the passage of an electrical current from anode towards cathode called forward current: the diode behaves like a closed switch. Figure 2(b) shows that the dynamic resistance of the diode decreases linearly in logarithmic scale while the voltage increases. Thereafter, from different values of V_D, the obtained dynamic resistances R_D will be used as electric impedance loads Z_a of the connected Schottky diode to calculate the corresponding dispersion curves.

In the literature [37, 38], the impedance of a diode Z_D is expressed as:

$$Z_D = \frac{6}{g_t(j\omega\tau)^3}\left(1 - j\omega\tau + \frac{(j\omega\tau)^2}{2} - e^{-j\omega\tau}\right), \tag{6}$$

where ω is the pulsation, g_t is the low frequency conductance and τ is the transit time. For instance, the set of values $g_t = 10^{-2}\ \Omega^{-1}$ and $\tau = 2.10^{-3}$ s gives at the first order the reference value of $Z_D = 1/g_t = R_D = 100\ \Omega$ as illustrated in Figure 3. This complex electrical impedance can be written as $Z_D = R_D + jX_D$, where both the resistive part R_D and reactive part X_D are frequency dependant. Following the equation (6), the representation of the Argand diagram is shown in Figure 3 in good agreement with that of an alternative model proposed by Lue [39].

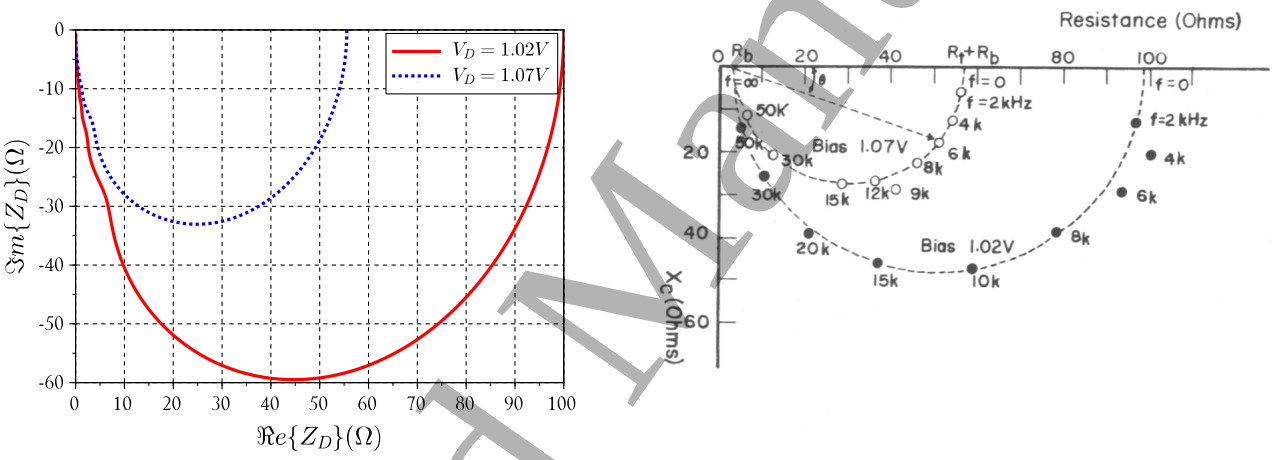

Figure 3: Diagram of Argand according to (a) equation (6) versus (b) Lue [39].

Despite this agreement in the low frequency range (Figure 3), this model of impedance for the diode (equation (6)) is very sensitive and not well defined in the studied MHz frequency range. Therefore, this study will focus only on the effect of the resistive part R_D of the impedance Z_D as defined in equation (5), with the standard data for a Schottky diode, summarized in Table 1.

3 Active control of PPC

3.1 *Theoretical model*

The considered multilayer structure is constituted of N stacks of 2 layers, alternating piezoelectric layer (Pz26) with electrodes and elastic layer (PMMA), denoted (piezoelectric/elastic)$\times N$. As illustrated in Figure 4, the studied configuration consists in connecting an external electrical impedance $Z_a^{(n)}$ driven by a voltage generator $U^{(n)}$ in parallel across the terminals of piezoelectric plates. The properties of the constituent materials are grouped together in Table 2 [29].

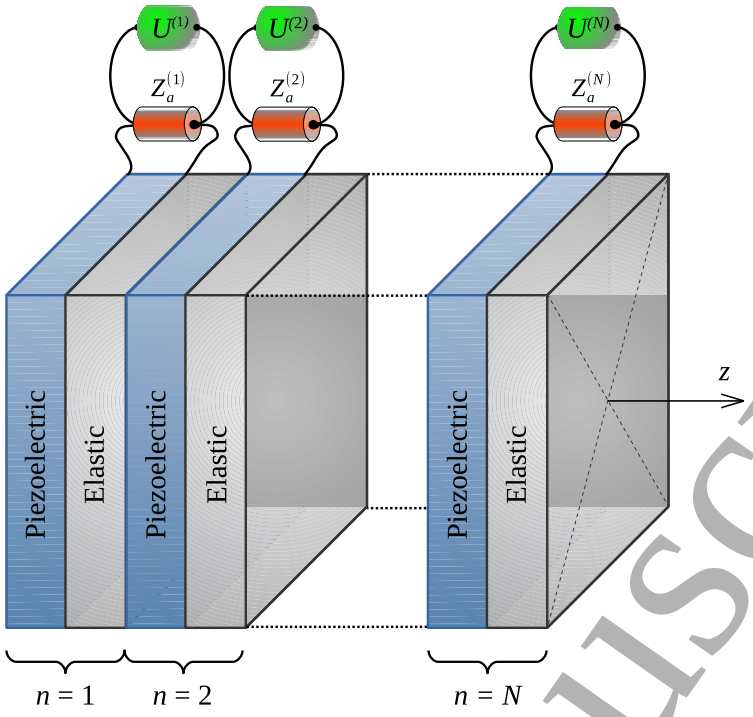

Figure 4: Geometry of the considered PPC.

Table 2: Elastic, piezoelectric and dielectric properties of the constitutive layers [19].

Material	h(mm)	ρ(kg/m^3)	c_L(m/s)	C_{33}^D(GPa)	h_{33}(GV/m)	β_{33}^s(Gm/F)	δ_m(%)	δ_e(%)
PMMA	4.13	1142	2744	8.6	-	-	0.028	-
Pz26	1.00	7700	4523	158	2.37	0.141	0.8	0.10

h: thickness; ρ: density; c_L: longitudinal velocity; C_{33}^D: elastic constant; h_{33}: piezoelectric constant; β_{33}^s: dielectric permeability constant at constant strain; δ_m: mechanical losses; δ_e: dielectric losses.

3.2 *Dispersion relation*

As illustrated in Figure 4, the presented PPC is made of a pattern based on an elementary unit cell, repeated from $n = 1$ to N, where N is the considered number of period. The basic unit cell is composed of a stack alternating piezoelectric and elastic plates having thicknesses h_1 and h_2, respectively. Based of one-dimensional propagation assumption, the solution of the equation of motion for the active layer $u_{3,1}(z)$ and for the elastic layer $u_{3,2}(z)$ gives the displacements in each layer i ($i = 1, 2$) where the subscript "3" refers both to the polarization axis and to the direction of propagation z:

$$\begin{cases} u_{3,1}(z) = a_1 \cos k_1(z) + b_1 \sin k_1(z), \\ u_{3,2}(z) = a_2 \cos k_2(z) + b_2 \sin k_2(z), \end{cases} \tag{7}$$

where a_i and b_i are unknown amplitudes, $k_i = \omega / c_{L,i}$ is the wavenumber in each plate with $\omega = 2\pi f$ the pulsation and $c_{L,i} = \sqrt{C_{33,i}/\rho_i}$ is the speed of the longitudinal waves.
For the piezoelectric layer ($i = 1$), the equations of piezoelectricity give

$$\begin{cases} \sigma_{3,1}(z) = C_{33}^D S_{3,1}(z) - h_{33} D_3(z), \\ E_3(z) = -h_{33} S_{3,1}(z) + \beta_{33}^s D_3(z), \end{cases} \tag{8}$$

where $\sigma_3(z)$ and $E_3(z)$ are stress and electric field, S_3 and D_3 are elastic strain and electric displacement, respectively. The constants C_{33}^D, h_{33} and β_{33}^s ($\beta_{33}^s = 1/\varepsilon_{33}^s$) are the elastic, piezoelectric and dielectric constants, respectively. The exponents D on C_{33}^D and S on β_{33}^s signify a constant displacement D and a constant deformation S, respectively. In the case of an elastic layer ($i = 2$), the dielectric effect is neglected ($E_3 = 0$) and equation (8) reduce to $\sigma_{3,2}(z) = C_{33,2}S_{3,2}(z)$ such that :

$$\sigma_{3,2}(z) = C_{33,2}(-k_2 a_2 \sin k_2(z) + k_2 b_2 \cos k_2(z)). \tag{9}$$

In the same way, as demonstrated by S. Degraeve *et al.* in [20] for the piezoelectric layer, the effect of the connected electric impedance load Z_a is taken on the expression of the electric displacement $D_3(z)$ as follows

$$D_3(Z_a) = \frac{h_{33}}{\beta_{33}^s h_1 (1 + j\omega C_0 Z_a)} \left(u_{3,1}(h_1) - u_{3,1}(0)\right). \tag{10}$$

As demonstrated by Degraeve *et al.* [20], the classical Hooke's law $\sigma_3 = C_{33}^D S_3$ is therefore modified through the contribution α due to the piezoelectric effect (h_{33} coefficient), itself involving the added electrical impedance Z_a in parallel to the piezoelectric layer. Thus, inserting equation (10) into (8) and after some arrangements, we obtain

$$\sigma_{3,1}(z) = C_{33}^D \left(S_{3,1}(z) - \alpha k_1 (u_{3,1}(h_1) - u_{3,1}(0))\right), \tag{11}$$

with $\alpha = k_t^2 / \left(k_1 h_1 \left(1 + j\omega C_0 Z_a\right)\right)$ the coupling piezoelectric coefficient, $k_t^2 = h_{33}^2/(C_{33}^D \beta_{33}^s)$ the piezoelectric thickness coupling coefficient, $C_0 = A/(\beta_{33}^s h_1)$ the clamped capacitance of the piezoelectric plate and A the electrode area.

Since, the considered PPC has a periodic pattern in its structure, the case where $Z_a^n = Z_a$ is considered for each of stack. Therefore, the boundary conditions are described through the continuity relations of the fields applied on the unit cell (Figure 4) and the periodicity using the Bloch-function $\chi = e^{jk(h_1+h_2)}$:

$$\begin{cases} u_{3,1}(h_1) = u_{3,2}(0), \\ \sigma_{3,1}(h_1) = \sigma_{3,2}(0), \end{cases} \quad \text{and} \quad \begin{cases} u_{3,1}(0) = \chi u_{3,2}(h_2), \\ \sigma_{3,1}(0) = \chi \sigma_{3,2}(h_2). \end{cases} \tag{12}$$

The application of boundary and continuity conditions using equations (7), (9), (11) and Bloch-Floquet function allow to construct the matrix system of which the dispersion relation is given by setting the determinant of the system to zero, this yields to the dispersion relation of the ultrasonic waves

$$\cos kh = \frac{c_1 c_2 - \frac{1}{2}\left(\delta + \frac{1}{\delta}\right) s_1 s_2 + \alpha\left(\delta s_2 (1 - c_1) - c_2 s_1\right)}{1 - \alpha s_1}, \tag{13}$$

where $h = (h_1 + h_2)$, $\delta = C_{33}^D k_1/(C_{33,2} k_2)$, $c_1 = \cos k_1 h_1, c_2 = \cos k_2 h_2, s_1 = \sin k_1 h_1$ and $s_2 = \sin k_2 h_2$. This relation (equation (13)) allows to establish the dispersion curves of the structure by taking into account the effect of the diode electrical impedance load $Z_a = Z_D$) applied to the terminals of the piezoelectric layers.

4 Results

In this section, according to electrical boundary conditions, dispersion curves are plotted thanks to the relationship given by equation (13). The theoretical calculation is performed using geometric and physical properties of the constitutive layers summarized in Table 2 and the diode properties in Table 1.

4.1 *Dispersion curves of (Pz26/PMMA) PPC*

The dispersion curves of a (Piezo/passive) PPC have been calculated according to equation (13). Those results have been compared and validated on the basis of the (Pz26/PMMA) PPC configuration depicted in the work of S.A. Mansoura *et al.* [17], in the case of short-circuit load ($Z_a = 0$), and an open-circuit load ($Z_a = +\infty$). Following this validation stage, as illustrated in Figure 5, the dispersion curves of (Pz26/PMMA) PPC are studied according to the dynamic resistance of the diode R_D connected to the electrodes of the Pz26 plate.

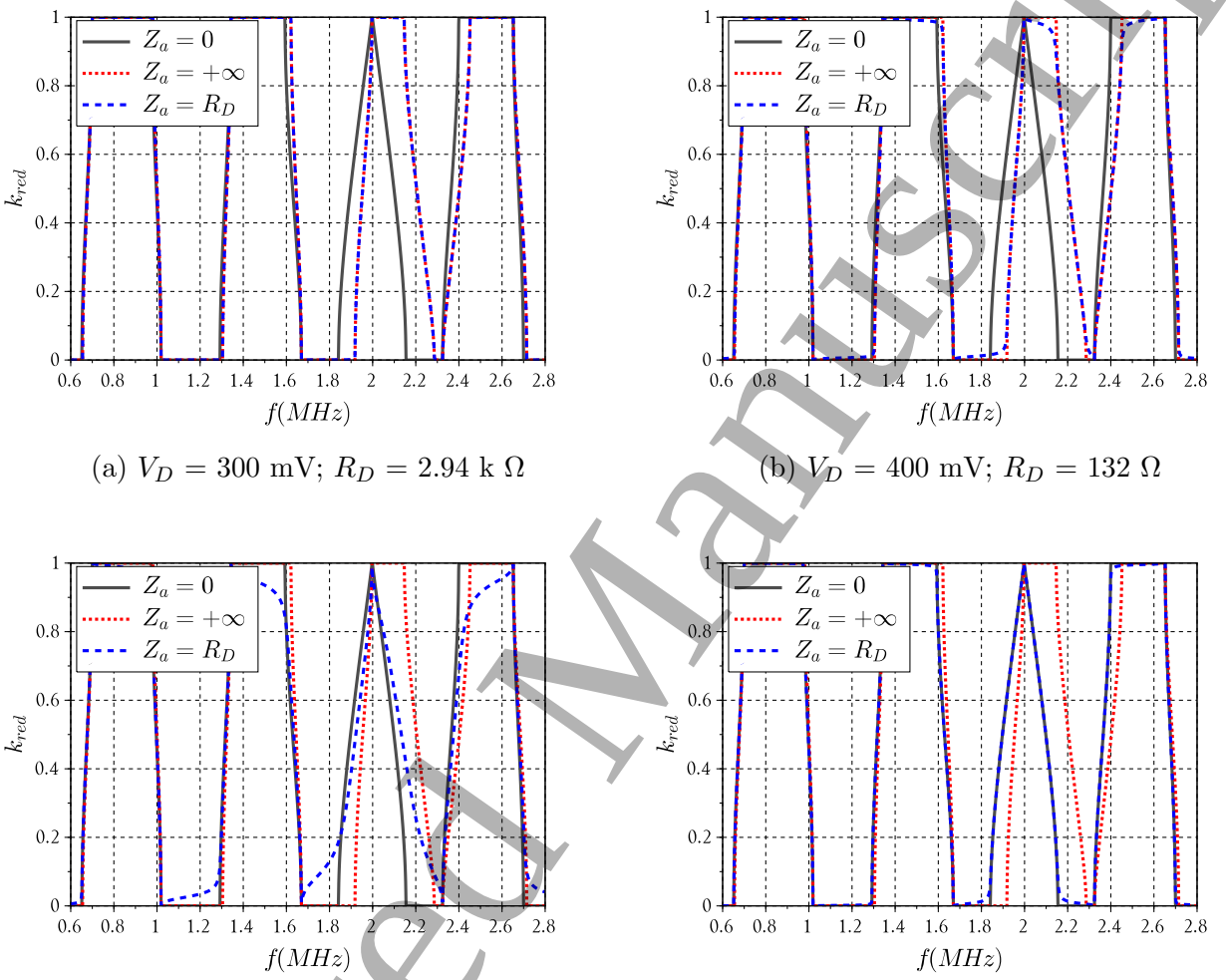

(a) $V_D = 300$ mV; $R_D = 2.94$ k Ω

(b) $V_D = 400$ mV; $R_D = 132$ Ω

(c) $V_D = 500$ mV; $R_D = 6$ Ω

(d) $V_D = 600$ mV; $R_D = 0.3$ Ω

Figure 5: Dispersion curves of (Pz26/PMMA) PPC for three electric boundary conditions: (black) short-circuit, (red) open-circuit and (blue) loaded by a dynamic resistance according to diode voltage: (a) $V_D = 300$ mV; (b) $V_D = 400$ mV; (c) $V_D = 500$ mV; (d) $V_D = 600$ mV.

It is shown that, while the value of the dynamic resistance of the diode decreases with respect to the voltage V_D which is function of current I_D, the dispersion profiles are modified. However, the dispersion profiles are practically the same for high dynamic resistance of the diode (Figure 5(a) and (b)), *i.e.* the dynamic resistance of the diode is still too high. Nevertheless, the modification of the dispersion curves can be observed for weaker values of the dynamic resistance of the diode (Figure 5(c) and (d)).

The analysis of the evolution of the bandwidths and forbidden bands allows to show the interest of

the diode like component to control an impedance in voltage. For instance, the analysis of Figure 5 shows that the addition of a resistive impedance load electrically in parallel with the piezoelectric material induces changes in the theoretical band structure different from the case where active layer is in short-circuit. However, it is reliable in this case to note that the dispersion curves when Pz26 is in open-circuit or loaded by a the resistance of diode are merged (Figure 5(a)). Thus, a shift in the position of different pass and forbidden bands is observed over a frequency band ranging from 1.83 to 2.45 MHz (Figure 5(a)). Outside this frequency range, whole dispersion curves are nearly identical. Theoretically, the widening of the gap is characterized: we observe the increase of the forbidden bands in the frequency ranges [1.83;1.91] MHz and [1.99; 2.15] MHz when the Pz26 layer is loaded by a diode which behaves like a resistance, while in short-circuit, pass bands were awaited. Contrary to what is observed previously, in [2.39; 2.45] MHz frequency range, we obtain the appearance of a slight bandwidth, initially prohibited in short-circuit. In the frequency range [1.83; 2.45] MHz, the obtained shift of the stop or pass bands is due to the existence of a strong electromechanical coupling between piezoelectric layer and the propagating ultrasonic waves. This shift can also be interpreted by the modification of the ultrasonic effective velocities in the piezoelectric layer when the resistance of a diode is connected.

4.2 *Effective parameters of the loaded Pz26 piezoelectric plate*

The connection of an electrical impedance to the terminals of the electrodes of the piezoelectric layer makes it possible to consider a modification of its effective elastic properties. To explain this modification, we write Hooke's relation for a piezoelectric plate by taking the effect of electrical boundary conditions. Thus, depending on the thickness mode, the Hooke's relation (equation (8)) is modified by the induced contribution of the piezoelectric coupling coefficient α. The stresses at the interfaces of the electrodes of the piezoelectric plate are then

$$\begin{cases} \sigma_{3,1}(0) = C_{33}^{D} S_{3,1}(0) - \alpha \left(u_{3,1}(h_1) - u_{3,1}(0)\right), \\ \sigma_{3,1}(h_1) = C_{33}^{D} S_{3,1}(h_1) - \alpha \left(u_{3,1}(h_1) - u_{3,1}(0)\right), \end{cases} \tag{14}$$

and the expressions of displacements and deformations at the same interfaces are written

$$\begin{cases} u_{3,1}(0) = a_1 + b_1, \\ u_{3,1}(h_1) = a_1 e^{jk_1h_1} + b_1 e^{-jk_1h_1}, \end{cases} \tag{15}$$

$$\begin{cases} S_{3,1}(0) = jk_1(a_1 - b_1), \\ S_{3,1}(h_1) = jk_1(a_1 e^{jk_1h_1} - b_1 e^{-jk_1h_1}). \end{cases} \tag{16}$$

The insertion of equation (15) and (16) into (14) allows to establish the following matrix system

$$\begin{pmatrix} \sigma_{3,1}(0) \\ \sigma_{3,1}(h_1) \end{pmatrix} = C_{33}^{D} \begin{pmatrix} 1-\alpha_{eff} & -\alpha_{eff} \\ -\alpha_{eff} & 1-\alpha_{eff} \end{pmatrix} \begin{pmatrix} S_{3,1}(0) \\ S_{3,1}(h_1) \end{pmatrix}, \tag{17}$$

with

$$\alpha_{eff} = \alpha \frac{1-c_1}{k_1 s_1} = \frac{k_t^2 \tan(k_1h_1/2)}{k_1h_1(1+Z_a/Z_0)}, \tag{18}$$

Equation (17) permits to deduce that the stress on an interface is proportional to the deformation on this same interface through an effective stiffness and the related effective longitudinal velocity by, respectively:

$$\begin{cases} C_{33,eff}^{D} = C_{33}^{D}(1-\alpha_{eff}), \\ c_{L,eff} = \sqrt{C_{33}^{D}(1-\alpha_{eff})/\rho}. \end{cases} \tag{19}$$

Figure 6(a) to (d) illustrate the effective modulation $\Re e\{\alpha_{eff}\}$ of the Pz26 piezoelectric plate according to the EBCs: short-circuit ($Z_a = 0$), open-circuit ($Z_a = +\infty$) and loaded by a diode ($Z_a = R_D$), depending on the applied DC voltage, *i.e.* (a) $V_D = 300$ mV; (b) $V_D = 400$ mV; (c) $V_D = 500$ mV; (d) $V_D = 600$ mV, respectively. Figure 6(a) shows that, when Pz26 is loaded by a diode of the resistance value equal $3k\Omega$, it operates practically like when it is in open-circuit, then the calculated effective modulation coefficient $\Re e\{\alpha_{eff}\}$ is constant, proving a weak coupling between the acoustic wave and the Pz26 electric quantities, different from the case where Pz26 is in short-circuit. This difference is more noticeable in the vicinity of the fundamental resonance frequency of the piezoelectric plate estimated around 2.26 MHz where an abrupt variation of the equivalent modulation coefficient $\Re e\{\alpha_{eff}\}$ is observed in short-circuit. Thus, for $R_D = 0.3$ Ω and $R_D = 2.94$ k Ω, it is observed that the coefficient $\Re e\{\alpha_{eff}\}$ varies between that of the open-circuit and that of the short-circuit electrical load. These values therefore determine the edges from which there is no longer any noticable variation due to the tunability of the PPC with a Schottky diode.

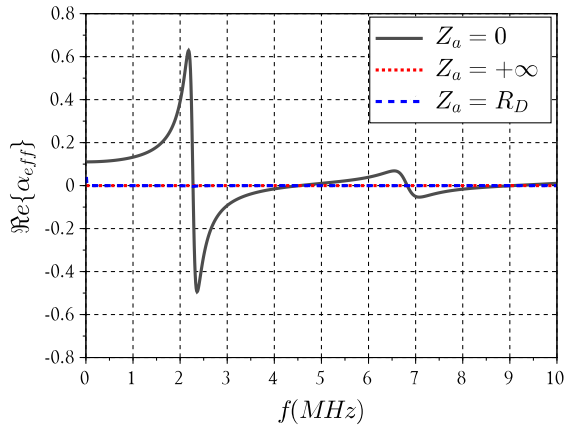

(a) $V_D = 300$ mV; $R_D = 2.94$ k Ω

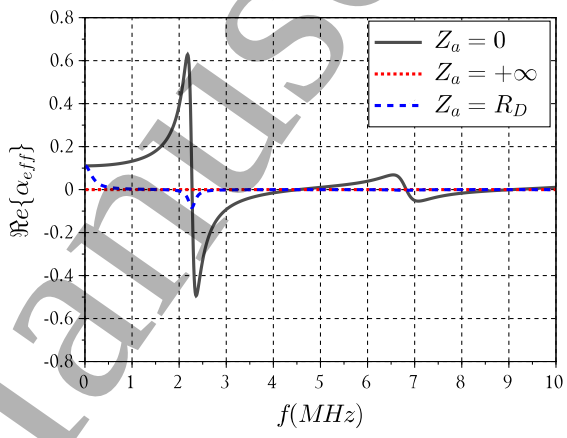

(b) $V_D = 400$ mV; $R_D = 132$ Ω

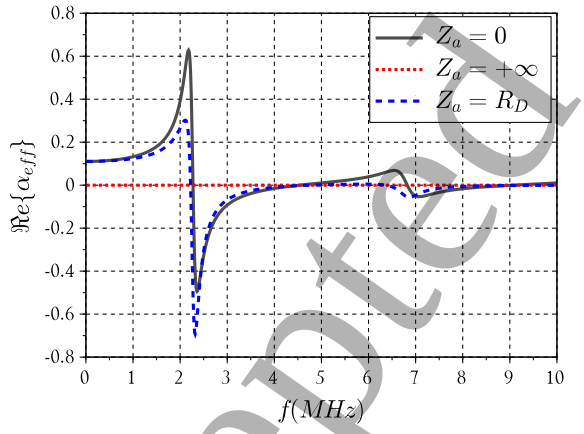

(c) $V_D = 500$ mV; $R_D = 6$ Ω

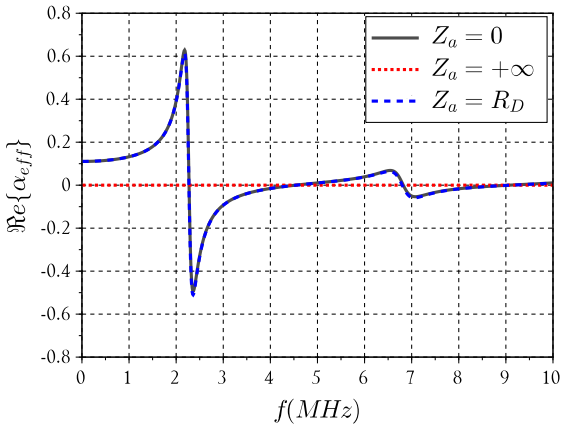

(d) $V_D = 600$ mV; $R_D = 0.3$ Ω

Figure 6: Effective modulation coefficient $\Re e\{\alpha_{eff}\}$ of Pz26 for various loads: short-circuit (black), open-circuit (red) and loaded by a diode (blue) under voltage: (a) $V_D = 300$ mV; (b) $V_D = 400$ mV; (c) $V_D = 500$ mV; (d) $V_D = 600$ mV.

In Figure 7 the evolution of the effective velocity $c_{L,eff}$ is illustrated for the Pz26 piezoelectric

plate according to the three considered EBCs: short-circuit ($Z_a = 0$), open-circuit ($Z_a = +\infty$) and loaded by a diode ($Z_a = R_D$), depending on the applied DC voltage, *i.e.* (a) $V_D = 300$ mV; (b) $V_D = 400$ mV; (c) $V_D = 500$ mV; (d) $V_D = 600$ mV, respectively. It is noticeable that, the effective velocity profiles change while increasing V_D when the Pz26 plate is loaded by a diode, corresponding to the decrease of R_D. From $V_D = 600$mV, the effective modulation coefficient $\Re e\{\alpha_{eff}\}$ (Figure 6) and effective velocity (Figure 7) profiles are completely merged to those of short-circuit, meaning that the diode connected to the Pz26 plate behaves like when Pz26 is short-circuited. Whereas, in open-circuit or in short-circuit, whatever the V_D value, the effective property profiles remain steadfast. Thus, depending on the V_D value, the connected diode, which behaves like an electrically driven impedance load, induces a significant variation of the effective modulation coefficient $\Re e\{\alpha_{eff}\}$ and effective velocity $\Re e\{c_{L,eff}\}$ in the piezoelectric plate.

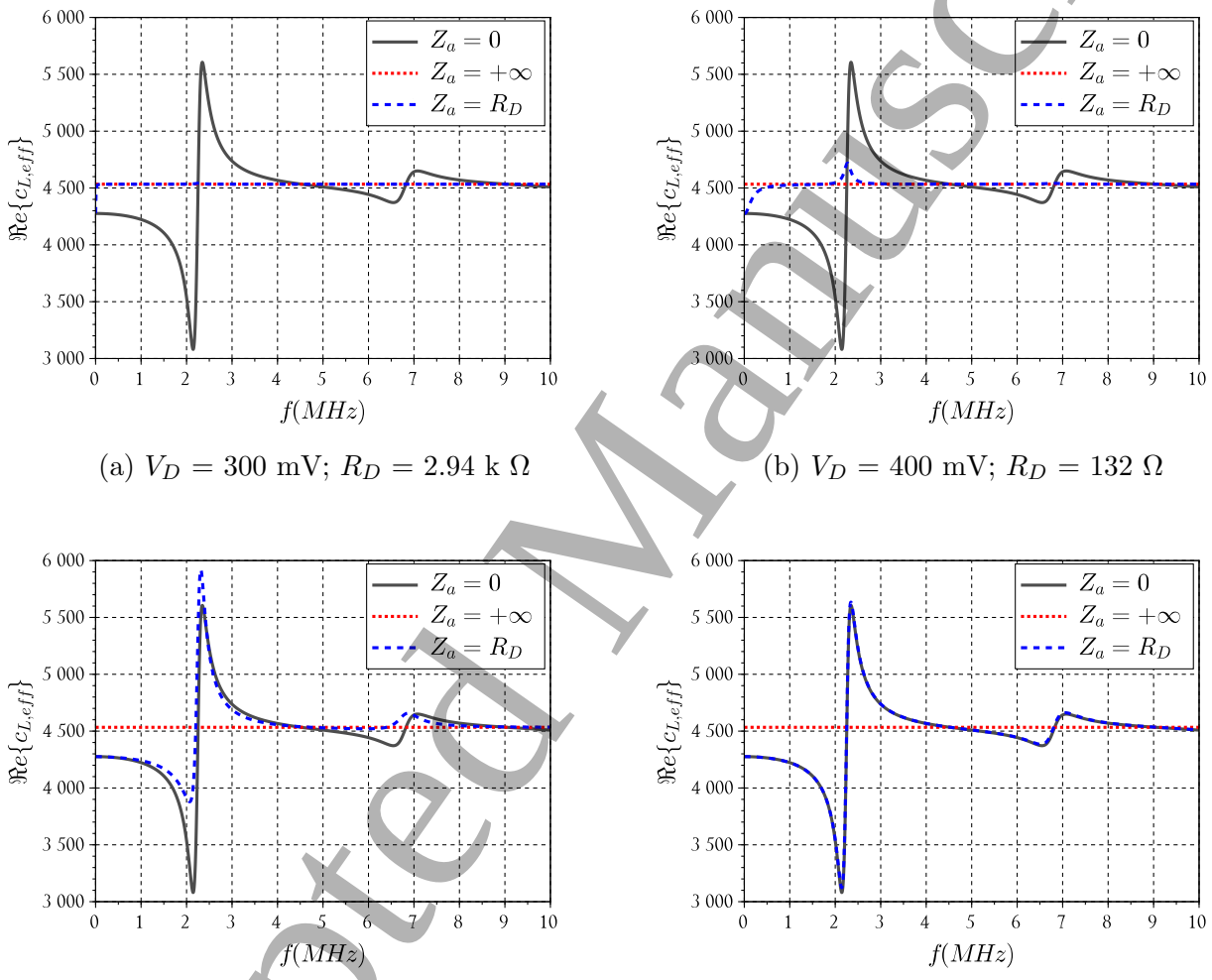

(a) $V_D = 300$ mV; $R_D = 2.94$ k Ω (b) $V_D = 400$ mV; $R_D = 132$ Ω

(c) $V_D = 500$ mV; $R_D = 6$ Ω (d) $V_D = 600$ mV; $R_D = 0.3$ Ω

Figure 7: Effective velocity $c_{L,eff}$ of Pz26 for various loads: short-circuit (black), open-circuit (red) and loaded by a diode (blue) under voltage: (a) $V_D = 300$ mV; (b) $V_D = 400$ mV; (c) $V_D = 500$ mV; (d) $V_D = 600$ mV.

Considering the dispersion curve of (Pz26/PMMA) piezoelectric phononic crystal (Figure 8(a)), we calculate and deduce the effective group velocity $c_{g,eff}$ of waves (Figure 8(b)) thanks to the following relation:

$$c_{g,eff} = \frac{\partial \omega}{\partial k_p}. \tag{20}$$

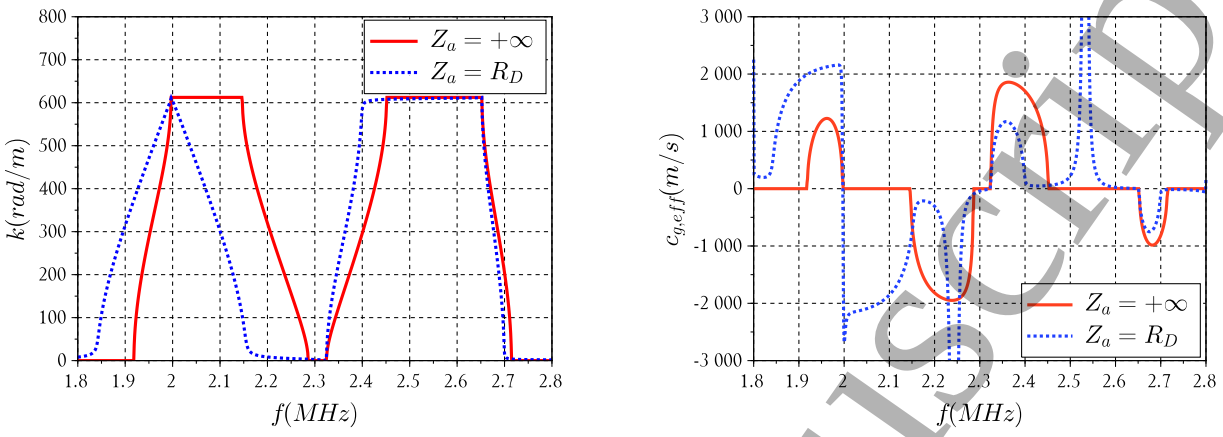

(a) (b)

Figure 8: (a) dispersion curve of Pz26/PMMA taking into account the effective velocity in Pz26 plate. (b) effective group velocity compared between open-circuit ($Z_a = +\infty$) and loaded by a diode ($Z_a = R_D = 0.3\ \Omega$).

As illustrated in Figure 8 (a), the passbands and stopbands are shifted when an electric load is applied to the Pz26 layer. The effective group velocity $c_{g,eff}$ can be deduced from equation (20) and is illustrated in Figure 8 (b). In-between the stopbands, the propagative modes values of velocities are resulting from a mixing law of the properties of the constitutive media (Pz26/PMMA) and the electric load applied to the Pz26 piezoelectric layer. As a consequence, the propagative modes are identified for the open-circuit ($Z_a = +\infty$) configuration for $f \in [1.92; 2.00] \cup [2.15; 2.28] \cup [2.32; 2.45] \cup [2.65; 2.71]$ MHz. Those propagative modes are shifted for the diode load ($Z_a = R_D = 0.3\ \Omega$) configuration, in which case they are observed for $f \in [1.84; 1.99] \cup [2.00; 2.15] \cup [2.32; 2.40] \cup [2.65; 2.70]$ MHz.

5 Conclusion

This study was related to the development of a piezoelectric phononic crystal that is able to generate and control the propagation of acoustic waves in specific frequency ranges called band gaps, thereby offering tunability of the phononic band structure. Interaction between waves and piezoelectric layers has first attracted our attention. The existence and the effect of an electromechanical coupling obtained by connecting the phononic structure to a nonlinear electrical component (Schottky diode) are examined in detail. We have pointed out that, depending of the diode resistance value, by alternating the periodic electric boundary conditions (short-circuiting, connecting to a diode) by an external control, one showed numerically the opening and/or the closing of a Bragg gap or hybridization gab in the PPC bands structure different from the case of open-circuit. Thus, the proposed tunable PPC in this study may be useful as an adaptation layer for the development of ultrasonic transducers. As aim of our forthcoming work, we target to study the assembly of the stiffness matrices for a bilayer, in order the obtain effective properties.

6 Appendix

The longitudinal waves propagation is governed by the Newton's law and the solution of this equation gives the displacement $u_{3,i}(z)$ in each layer i ($i = 1;\ 2$) as a function of the position z along the propagation direction indicated by the subscript "3" on the equations. In each layer, displacement and strain relations are respectively given by:

$$\begin{cases} u_{3,i}(z) = a_i \cos(k_i z) + b_i \sin(k_i z) \\ S_{3,i}(z) = -k_i a_i \sin(k_i z) + k_i b_i \cos(k_i z) \end{cases} \tag{21}$$

that is

$$\begin{cases} u_{3,1}(z) = a_1 \cos(k_1 z) + b_1 \sin(k_1 z) \\ u_{3,2}(z) = a_2 \cos(k_2 z) + b_2 \sin(k_2 z) \end{cases} \tag{22}$$

and

$$\begin{cases} S_{3,1}(z) = -k_1 a_1 \sin(k_1 z) + k_1 b_1 \cos(k_1 z) \\ S_{3,2}(z) = -k_2 a_2 \sin(k_2 z) + k_2 b_2 \cos(k_2 z) \end{cases} \tag{23}$$

For the piezoelectric layer ($i = 1$), the equations of piezoelectricity give

$$\begin{cases} \sigma_{3,1}(z) = C_{33}^D S_{3,1}(z) - h_{33} D_3(z) \\ E_3(z) = -h_{33} S_{3,1}(z) + \beta_{33}^S D_3(z) \end{cases} \tag{24}$$

In the case of an elastic layer ($i = 2$), the dielectric effect is neglected ($E_3 = 0$) and the stress is given by the Hook's law $\sigma_{3,2}(z) = C_{33,2} S_{3,2}(z)$ such that

$$\sigma_{3,2}(z) = C_{33,2} \left(-k_2 a_2 \sin(k_2 z) + k_2 b_2 \cos(k_2 z)\right) \tag{25}$$

In the same way, as demonstrated by Degraeve *et al.* [20] for the piezoelectric layer, the effect of the connected electrical impedance load Z_a is taken into account in the expression of the electrical displacement $D_3(Z_a)$ as follows:

$$D_3(Z_a) = \frac{h_{33}}{\beta_{33}^S h_1 (1 + j\omega C_0 Z_a)} \left(u_{3,1}(h_1) - u_{3,1}(0)\right) \tag{26}$$

The detailed process for the calculation of the expression of the electrical displacement $D_3(Z_a)$ is related to the electrical field E_3, itself linked to the electrical potential by: $E_3 = -grad(V)$.

The voltage across both electrode faces of the piezoelectric plate is written:

$$V = Z_a I = -\int_0^{h_1} E_3 dz \tag{27}$$

Knowing that the current I derives from the electrical displacement D_3

$$I = A \frac{\partial D_3}{\partial t}, \tag{28}$$

where $D_3 = D_0 e^{j\omega t}$ *i.e.* $I = j\omega A D_3$.

Combining equations (27) and (28) gives

$$j\omega Z_a A D_3 = -\int_0^{h_1} E_3 dz \tag{29}$$

Inserting equation (24) into equation (29) yields

$$j\omega Z_a A D_3 = h_{33} \int_0^{h_1} S_{3,1}(z) dz - \beta_{33}^S \int_0^{h_1} D_3 dz \tag{30}$$

According to the Gauss's law applied on the thickness of active plate, the electrical displacement $D_3(z)$ is uniform along the direction of propagation, that is

$$\mathrm{div}(D_3) = \frac{\partial D_3}{\partial z} = 0, \tag{31}$$

i.e. D_3 is constant, and equation (31) can be rewritten as

$$j\omega Z_a A D_3 = h_{33}\left[u_{3,1}(z)\right]_0^{h_1} - \beta_{33}^S [D_3(z)]_0^{h_1} = h_{33}(u_{3,1}\left(h_1\right) - u_{3,1}(0)) - \beta_{33}^S D_3 h_1 \tag{32}$$

i.e.

$$j\omega Z_a A D_3 + \beta_{33}^S D_3 h_1 = h_{33}(u_{3,1}\left(h_1\right) - u_{3,1}(0)) \tag{33}$$

i.e.

$$D_3(Z_a) = \frac{h_{33}(u_{3,1}(h_1) - u_{3,1}(0))}{j\omega Z_a A + \beta_{33}^S h_1} = \frac{h_{33}}{\beta_{33}^S h_1 (1 + \frac{j\omega Z_a A}{\beta_{33}^S h_1})}(u_{3,1}\left(h_1\right) - u_{3,1}(0)) \tag{34}$$

where $C_0 = A/(\beta_{33}^S h_1)$, hence retrieving the expression of equation (26).

References

[1] E. Yablonovitch, Inhibited spontaneous emission in solid-state physics and electronics, *Phys. Rev. Lett.*, vol. 58, pp. 2059-2060, 1987.

[2] A. Khelif, A. Choujaa, S. Benchabane, B. Djafari-Rouhani, and V. Laude, Experimental study of guiding and filtering of acoustic waves in a two dimensional ultrasonic crystal, *Zeitschrift für Kristallographie*, vol. 220, p. 836, 2005.

[3] P. Maréchal, L. Haumesser, L.P. Tran-Huu-Hue, J. Holc, D. Kuscer, M. Lethiecq, and G. Feuillard, Modeling of a high frequency ultrasonic transducer using periodic structures, *Ultrasonics*, vol. 48, pp. 141-149, 2008.

[4] F. Wu, Z. Liu, and Y. Liu, Acoustic band gaps created by rotating square rods in a two-dimensional and lattice, *Physical Review*, vol. 66, p. 046628, 2002.

[5] F. Casadei, T. Delpero, A. Bergamini, P. Ermanni, and M. Ruzzene, Piezoelectric resonator arrays for tunable acoustic wave guides and metamaterials, *J. Appl. Phys.*, vol. 112, p. 064902, 2012.

[6] K.L. Jim, C.W. Leung, S.T. Lau, S.H. Choy, and H.L.W. Chan, Thermal tuning of phononic band structure in ferroelectric ceramic/epoxy phononic crystal, *Applied Physics Letters*, vol. 94, p. 193501, 2009.

[7] G. Wang, S.B. Chen, and J.H. Wen, Broadband attenuation in Phononic Beams induced by periodic arrays of feedback shunted piezoelectric patches, *Chin. Phys. Lett.*, vol. 29, p. 064302, 2012.

[8] J.F. Robillard, O. Boumatar, J.O. Vasseur, P.A. Deymier, M. Stippinger, A.C. Hladky-Hennion, Y. Pennec, and B. Djafari-Rouhani, Tunable magnetoelastic phononic crystals, *Applied Physics Letters*, vol. 95, p. 124104, 2009.

[9] V. Pashchenko, Surface acoustic wave ferroelectric phononic crystal tunable by electric field, *Nanosystems: Physics, Chemistry, Mathematics*, vol. 4, pp. 630-634, 2013.

[10] J. Robillard, O. Bou-Matar, J.O. Vasseur, P. Deymier, M. Stippinger, A.C. Hladky-Hennion, Y. Pennec, and B. Djafari-Rouhani, Tunable magnetoelastic phononic crystals, *Applied Physics Letters*, vol. 95, p. 124104, 2009.

[11] A. Bayat and F. Gordaninejad, A magnetically field-controllable phononic crystal, *Proceedings of the SPIE*, vol. 9057, p. 905713, 2014.

[12] S. Degraeve, C. Granger, B. Dubus, J.O. Vasseur, A.C. Hladky-Hennion, and M. Pham-Thi, Contrôle électrique de la propagation d'ondes élastiques dans des cristaux phononiques piézoélectriques, *21ème Congrès Français de Mécanique (CFM)*, Bordeaux, France, 2013.

[13] M. Lan and P. Wei, Band gap of piezoelectric/piezomagnetic phononic crystal with graded interlayer, *Acta Mechanica*, vol. 225, pp. 1779-1794, 2014.

[14] S. Alan, A. Allam, and A. Erturk, Programmable mode conversion and bandgap formation for surface acoustic waves using piezoelectric metamaterials, *Applied Physics Letters*, vol. 115, p. 093502, 2019.

[15] F.H. Chikh-Bled, N. Kherraz, R. Sainidou, P. Rembert, and B. Morvan, Piezoelectric phononic plates: retrieving the frequency band structure via all-electric experiments, *Smart Materials and Structures*, vol. 28, p. 115046, 2019.

[16] S.A. Mansoura, P. Benard, B. Morvan, P. Maréchal, A.C. Hladky-Hennion, and B. Dubus, Theoretical and experimental analysis of a piezoelectric plate connected to a negative capacitance at MHz frequencies, *Smart Materials and Structures*, vol. 24, p. 115032, 2015.

[17] S.A. Mansoura, P. Maréchal, B. Morvan, and B. Dubus, Analysis of a phononic crystal constituted of piezoelectric layers using electrical impedance measurement, *Physics Procedia*, pp. 283–286, 2015.

[18] C. Vasseur, C. Croënne, B. Dubus, J.O. Vasseur, A.C. Hladky-Hennion, C. Prévot, P. Martins, and M. Pham-Thi, Numerical and experimental demonstration of the electrical Bragg band gaps in piezoelectric plates with a periodic array of electrodes, *IEEE International Ultrasonics Symposium (IUS)*, pp. 1–4, 2017.

[19] L. Airoldi and M. Ruzzene, Design of tunable acoustic metamaterials through periodic arrays of resonant shunted piezos, *New Journal of Physics*, vol. 13, p. 113010, 2011.

[20] S. Degraeve, C. Granger, B. Dubus, J.O. Vasseur, M. Pham-Thi, and A.C. Hladky-Hennion, Bragg band gaps tunability in an homogeneous piezoelectric rod with periodic electrical boundary conditions, *Journal of Applied Physics*, vol. 115, p. 194508, 2014.

[21] S. Degraeve, C. Granger, B. Dubus, J.O. Vasseur, M.Pham-Thi, and A.C. Hladky-Hennion, Tunability of Bragg band gaps in one-dimensional piezoelectric phononic crystals using external capacitances, *Smart Materials and Structures*, vol. 24, p. 085013, 2015.

[22] S. Degraeve, C. Granger, B. Dubus, J.O. Vasseur, M. Pham-Thi, and A.C. Hladky-Hennion, Tunability of a one-dimensional elastic/piezoelectric phononic crystal using external capacitances, *Acta Acustica united with Acustica*, vol. 101, pp. 494–501, 2015.

[23] B. Dubus, M.F. Ponge, A.C. Hladky-Hennion, J. Vasseur, and M. Pham-Thi, Highly tunable Fabry-Perot resonators using piezoelectric phononic crystals, *IEEE International Ultrasonics Symposium (IUS)*, pp. 154–157, 2014.

[24] M.F. Ponge, B. Dubus, C. Granger, J.O. Vasseur, M. Pham-Thi, and A.C. Hladky-Hennion, Theoretical and experimental analyses of tunable Fabry-Perot resonators using piezoelectric phononic crystals, *IEEE Transactions on Ultrasonics, Ferroelectrics, and Frequency Control*, vol. 62, pp. 1114–1121, 2015.

[25] S.A. Mansoura, B. Morvan, P. Maréchal, A.C. Hladky-Hennion, and B. Dubus, Study of an hybridization gap in a one dimensional piezoelectric phononic crystal, *Physics Procedia*, pp. 279–282, 2015.

[26] E.A. Flores Parra, A. Bergamini, B. Lossouarn, B. Van Damme, M. Cenedese, and P. Ermanni, Bandgap control with local and interconnected LC piezoelectric shunts, *Applied Physics Letters*, vol. 111, p. 111902, 2017.

[27] Y. Zheng, J. Zhang, Y. Qu, and G. Meng, Investigations of a piezoelectric metastructure using negative-resistance circuits to enhance the bandgap performance, *Journal of Vibration and Control*, vol. 28, pp. 2346–2356, 2022.

[28] S.A. Mansoura, B. Morvan, P. Maréchal, P. Benard, A.C. Hladky-Hennion, and B. Dubus, Tunability of the band structure of a piezoelectric phononic crystal using electrical negative capacitance, *IEEE International Ultrasonics Symposium (IUS)*, 2015, pp. 1–4.

[29] P. Maréchal, Ultrasons et milieux complexes: matériaux viscoélastiques multicouches et interactions piézoélectriques, Habilitation à Diriger des Recherches, Université Le Havre Normandie, LOMC, UMR 6294 CNRS, 2019.

[30] S.V. Kalinin and D.A. Bonnell, Scanning impedance microscopy of an active Schottky barrier diode, *Journal of Applied Physics*, vol. 91, pp. 832-839, 2002.

[31] D. Eon, A. Traoré, J. Pernot, et E. Gheeraert, Recent progress on diamond Schottky diode, *in 28th International Symposium on Power Semiconductor Devices and ICs (ISPSD)*, pp. 55-58, 2016.

[32] B. Ozpineci and L.M. Tolbert, Characterization of SiC Schottky diodes at different temperatures, *IEEE Power Electron. Lett.*, vol. 1, pp. 54-57, 2003.

[33] J.L. Hesler and T.W. Crowe, Responsivity and Noise Measurements of Zero Bias Schottky Diode Detectors, *18th Intl. Symp. Space Terahertz Techn.*, 2007.

[34] J. Tausch, Computing Floquet-Bloch modes in biperiodic slabs with boundary elements, *Journal of Computational and Applied Mathematics*, vol. 254, pp. 192-203, 2013.

[35] D. Pardo, J. Grajal, C.G. Pérez-Moreno and S. Pérez, An Assessment of Available Models for the Design of Schottky-Based Multipliers up to THz Frequencies, *IEEE Trans. Terahertz Sci. Technol.*, vol. 4, p. 277-287, 2014.

[36] S.M. Sze and K.K. Ng, Semiconductor devices - Physics and Technology, John Wiley and Sons, 2006.

[37] J. Shao and G.T. Wright, Characteristics of the space-charge-limited dielectric diode at very high frequencies, *Solid-State Electron*, vol.3, pp. 291-303, 1961.

[38] A. Van der Ziel, Solid State Physical Electronics, Prentice-Hall, Englewood Cliffs, NJ, 1976.

[39] J.T. Lue, Junction impedance measurements of diodes by a simplified lock-in amplifier, *IEEE Transactions on Instrumentation and Measurement* , vol. 26, pp. 415-419, 1977.